Original Research

Parametric optimization of culture chamber for cell mechanobiology research

Xutong Guo[1,2], Ziqi Wang[1,2], Lilan Gao[1,2] and Chunqiu Zhang[1,2]

[1]Tianjin Key Laboratory for Advanced Mechatronic System Design and Intelligent Control, School of Mechanical Engineering, Tianjin University of Technology, Tianjin 300384, China; [2]National Demonstration Center for Experimental Mechanical and Electrical Engineering Education, Tianjin University of Technology, Tianjin 300384, China
Corresponding authors: Chunqiu Zhang. Email: zcqarticle@163.com; Lilan Gao. Email: gaolilan780921@163.com

Impact Statement

The improvement of the mechanical loading device in this article is the foundation of mechanobiological research since mechanical signals influence the morphology, function, differentiation, proliferation, and growth of cells. This article proposes a design and manufacturing scheme for a cell loading device, which effectively solves the problem of non-uniform strain in past experiments. With the innovative design of the culture chamber, researchers can more accurately study the responses of cells under strain loading. The innovative chamber provides a more reliable tool for cell mechanobiological research.

Abstract

Mechanical signals influence the morphology, function, differentiation, proliferation, and growth of cells. Due to the small size of cells, it is essential to analyze their mechanobiological responses with an *in vitro* mechanical loading device. Cells are cultured on an elastic silicone membrane substrate, and mechanical signals are transmitted to the cells by the substrate applying mechanical loads. However, large areas of non-uniform strain fields are generated on the elastic membrane, affecting the experiment's accuracy. In the study, finite-element analysis served as the basis of optimization, with uniform strain as the objective. The thickness of the basement membrane and loading constraints were parametrically adjusted. Through finite-element cycle iteration, the "M" profile basement membrane structure of the culture chamber was obtained to enhance the uniform strain field of the membrane. The optimized strain field of culture chamber was confirmed by three-dimensional digital image correlation (3D-DIC) technology. The results showed that the optimized chamber improved the strain uniformity factor. The uniform strain area proportion of the new chamber reached 90%, compared to approximately 70% of the current chambers. The new chamber further improved the uniformity and accuracy of the strain, demonstrating promising application prospects.

Keywords: Adherent cells, culture chamber, finite-element analysis, 3D-DIC, strain uniformity factor, optimized design

***Experimental Biology and Medicine* 2023; 248: 1708–1717. DOI: 10.1177/15353702231198079**

Introduction

As the smallest living activity unit in the human body, cells behavior is affected by various biological, chemical, and mechanical signals.[1,2] The mechanical signals continuously stimulate cells and trigger different behaviors regulating cell activities, such as growth, proliferation, and migration.[3–5] Studies have demonstrated that mechanical stimulation affects organ morphogenesis,[6] skeletal muscle differentiation,[7] and central nervous system development.[8] However, it is difficult to directly observe the mechanisms of cell mechanobiological responses due to the complexity of the *in vivo* environment, and the challenges also occur in studying cell responses in isolated animal tissues.[9] Therefore, researchers have turned to macro-scale investigations[10] to study cellular responses to mechanical stimulation through *in vitro* experiments.[11–13]

In mechanobiological studies, an appropriate loading system is crucial for simulating mechanical signals in the natural environment.[14] *In vitro* mechanical loading devices have been developed to study cell survival, differentiation, and proliferation.[15–17] These devices typically comprise driving, transmission, and culturing chamber modules. Cells are seeded onto the culturing chamber basement membrane, and mechanical stimulation is indirectly transferred to the cells via the membrane.[18–21] The culture chamber in the device, as a direct function module for delivering mechanical stimulation to cells, has garnered attention from researchers. The chamber can be a silicone membrane or a closed chamber with different loading conditions according to the device used to study specific biomechanical phenomena. The basement membrane is mainly round or rectangular,[22–25] with thicknesses ranging from 200 to 2000 μm, and other

dimensions of the chamber depend on the specific mechanical experiments. However, the experimental results are affected by the limited transfer force of the membrane, non-uniform strain distribution, and low accuracy of the strain field.[26,27]

The non-uniform strain field of the membrane is the key factor badly affecting the experimental results. In fact, the chamber's rectangular basement membrane elongates longitudinally while shortens laterally, resulting in different strains at various locations on the membrane. At the same time, mechanical signal-induced cell responses depend on strain magnitude,[28,29] which further increases the complexity of cell mechanobiological response. Researchers have devised multiple strategies, such as designing cylindrical or O-ring structures with flat-top surfaces that are concentric with a circular membrane[30–32] or reducing the thickness of the flexible basement.[33] However, the uniform strain of the basement membrane was not specifically quantified in the relevant studies. Therefore, the strain uniformity of the basement membrane needs to be studied by selecting a reasonable culture chamber structure.

In our previous experiments and studies, an "M" profile structured culture chamber was designed and optimized to enhance the strain uniformity area of the basement membrane (recommended for cell culture).[34] The proportion after optimization of the uniform strain area reached up to 70%, compared to 57% in the constant thickness membrane of chamber. In this article, culture chambers with two different elastic basement membrane thicknesses were designed using the finite-element optimization function, introduced strain uniformity factors, and further enhanced the strain uniformity area on the basement membrane. A self-designed cell loading device was used to examine the affects of mechanical loading on cultured cell growth. Three-dimensional digital image correlation (3D-DIC) was used to verify the strain field generated by the tensile of the culture chamber.

Materials and methods

Development of cell loading device

The cell loading device is based on the substrate deformation technique,[35] as shown in Figure 1. It consists of a drive control system, a power transmission system, and a cell culture system. The drive control system includes a stepper motor (model: 28BYJ-48, power: 800 W, stop accuracy: ± 0.05°) and a programmable controller, which can realize functions such as program writing, controlling displacement, zero position, and the number of cycles. In the power transmission system, the stepper motor is connected to the ball screw to generate a linear motion, and the end of the screw is connected to the telescoping platform where the culture chamber is placed. The cells adhering to the basement membrane are subjected to mechanical strain. The cell culture system consists of a culture chamber and medium. The chamber is made of medical type A and B silicone at a ratio of 1:1 and processed by vacuum, plasma cleaning, and ultrasonic cleaning.

Data determination of silicone material

The chamber is cast from a silicone rubber material, classified as a hyper-elastic material. To determine the material parameters as the basic data for finite-element analysis,[36] a tensile test must be conducted. The dumbbell-shaped specimen is shown in Figure 2, and its manufacturing method is consistent with the culture chamber. The dimensions in Figure 2(a) are $L_0 = 33$ mm and $S_0 = 18$ mm^2. It is assumed that the rubber material is isotropic, with large deformation and incompressible material. The uniaxial static experiment was conducted using an Electromagnetic Dynamic Mechanical Analysis System (M100, CARE). The tensile speed was 8.3 mm/s, and the tensile displacement from 1 to 10 mm. The average load–displacement data were obtained by repeated experiments three times, as shown in Figure 2(b). The stress–strain curve of the silicone material was derived using Equations (1) and (2), as shown in Figure 2(c), and the data were then imported into the finite-element software.

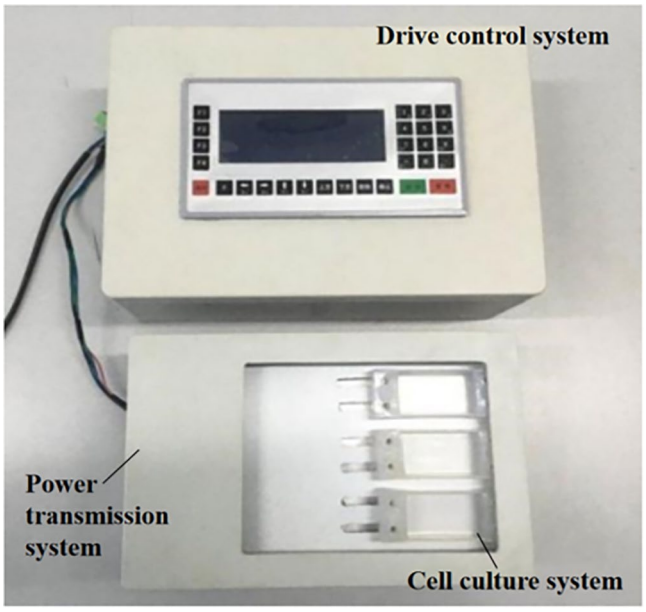

Figure 1. Development of a tensile loading device for adherent cells.

$$\varepsilon = \frac{\Delta L}{L_0} \tag{1}$$

ΔL is the axial deformation of the test piece, in mm, and L_0 is the original length of the specimen, in mm;

$$\sigma = \frac{P}{S_0}(1+\varepsilon) \tag{2}$$

P is the axial load on the tensile test piece, in N; S_0 is the initial cross-sectional area of the tensile test piece, in mm^2.

Optimization design of culture chamber

Structural optimization is an iterative solution process in which the finite-element model is modified several times. This iteration is based on a series of constraints to approach the set goal. The shape optimization function in the ABAQUS (SIMULIA, Paris, France) software was used for model design in this study. A condition-based algorithm was used to determine the optimized direction based on the solved results and update the design variables according to the constraints. The optimization area is the lower surface of the basement membrane, and the reference value in the

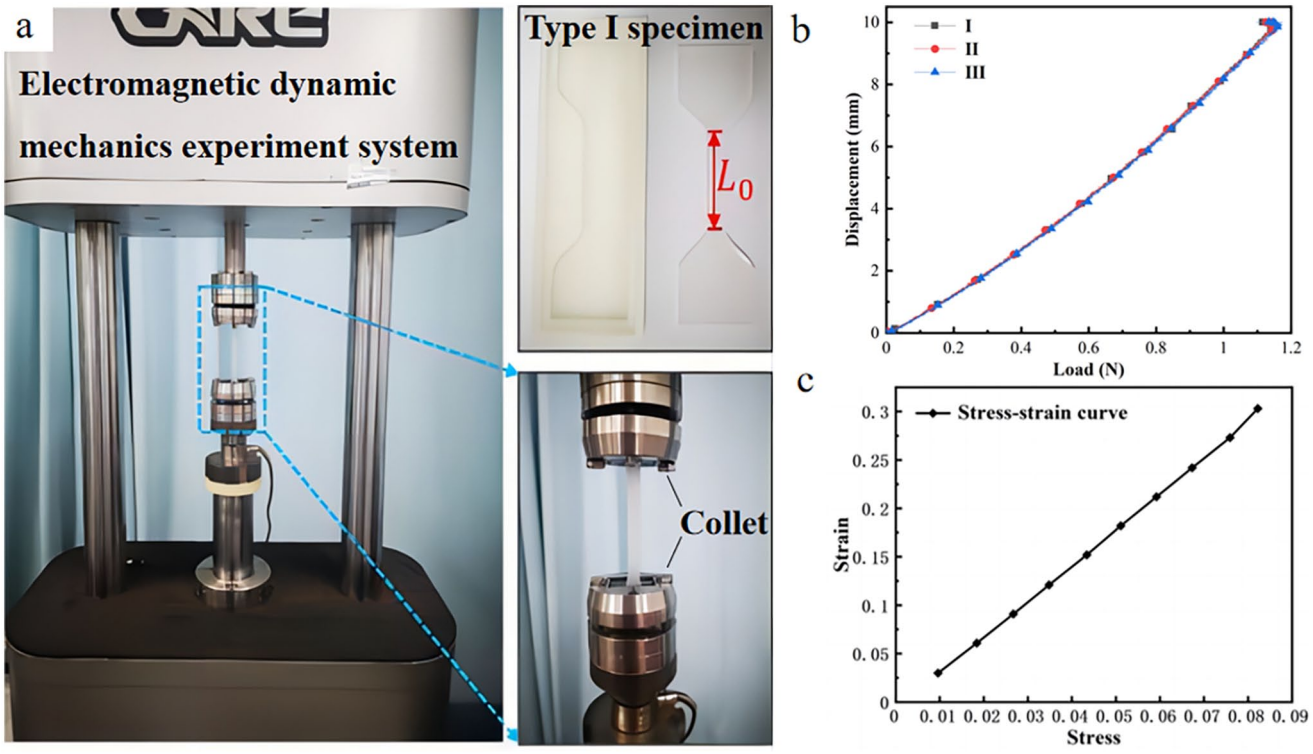

Figure 2. Specimen tensile test: (a) dumbbell I specimen was tested in a dynamic tensile machine; (b) three sets of tensile load displacement test data of the specimen under the same condition; and (c) stress-strain curve of specimen material properties.

objective function is the predetermined strain value, such as strain 1%, 5%, and 10%. The upper surface of the membrane is constrained, which does not change shape during the optimization process. The optimization variable is the basement membrane thickness (Tn), and the optimization objective is the maximum strain ε_{max}. The optimization can be expressed by the mathematical model, as follows in Equation (3):

$$\text{Obj1}: \text{Maximum} - \varepsilon_{\max}$$
$$T_{nmin} \le T_n \le T_{nmax} \tag{3}$$

The simulation is based on the condition that strain is applied to the loading pile. The model and meshing are shown in Figure 3. The culture chamber has a rectangular membrane with dimensions of 40 mm × 26.8 mm × 1 mm, and the material properties are selected from the Mooney–Rivlin strain potential energy; these parameters are the uniaxial tensile measured data of silicone material (Figure 2(c)). The chamber model uses C3D8R-type mesh, and the loading pile employs C3D10R-type mesh. The left loading pile is constrained, while the right is subjected to an outward strain of 1% to 10%. The basement membrane is optimized according to the strain distribution obtained from the simulation. Compared to the shape of the membrane after tensile strain, this optimization has a contour thickness profile. To quantify the strain uniformity on the membrane, a strain uniformity factor is introduced, as follows in Equation (4):

$$\gamma(x\%) = \frac{s(x\%)}{S} \tag{4}$$

In the Equation (4), S represents the total area of the basement membrane, and $s(x\%)$ represents the effective strain area, which the strain amplitude does not exceed $\pm x\%$ of the longitudinal strain amplitude at the center point of the membrane. The blue area is s, and the overall rectangular area is S, as shown in Figure 4. We use the IMAGE software to adjust the strain color cloud image to a gray image, and the strain uniformity factor is calculated. For example, if the longitudinal strain at the center point of the membrane is 1% and the area is 0.57572*S (the effective strain area), and the strain in this area ranges from 0.95% to 1.05%, then the strain uniformity coefficient $\gamma(5\%)$ is 0.57572. Under a given $x\%$, the larger the γ value, the higher the strain uniformity. As the chamber is longitudinally stretched, the value of γ strain represents the strain uniformity on the membrane.

As shown in Figure 5, our laboratory has previously optimized a double-column symmetrical structure culture chamber with a basement membrane thickness of 0.5 mm (Double-0.5 chamber). The strain uniformity factor has been raised from 0.57 to 0.70. There is still a possibility for improvement in the optimization. In the study, the thickness of the membrane was increased to 1 mm, as shown in Figure 6(a), resulting in a double-column symmetrical structure with a membrane thickness of 1 mm (Double-1 chamber). A single-column symmetrical structure with a membrane thickness of 0.5 mm (Single-0.5 chamber) was designed to simplify the machining process, as shown in Figure 6(b). The two structures were optimized to obtain strain uniformity factors and compared with the previous optimization results.

Experiment on 3D-DIC

The 3D-DIC experiment uses the XTDIC strain measurement and analysis system, which is an optical non-contact

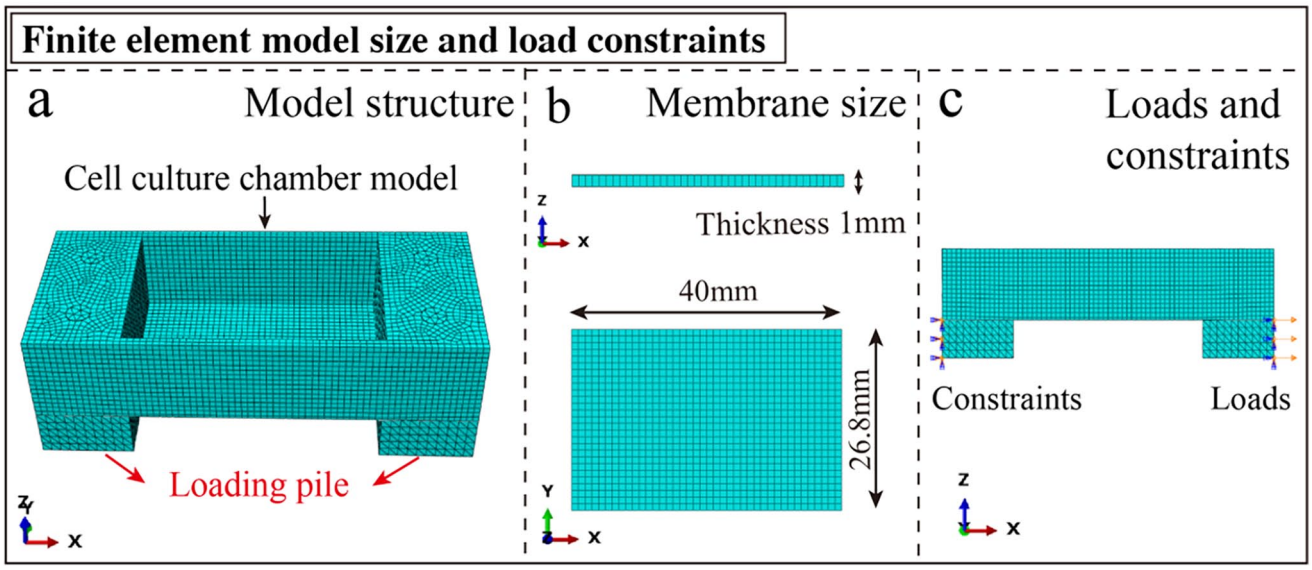

Figure 3. Finite-element model size and load constraints: (a) the model structure, (b) the membrane size, and (c) the loads and constraints.

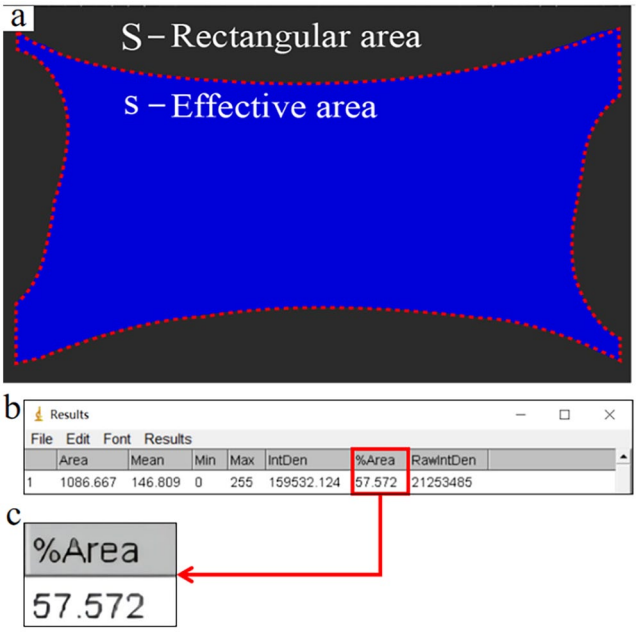

Figure 4. Expression of strain uniformity of basement membrane: (a) the ratio of effective strain area, (b) the strain uniformity factor is obtained to express the strain uniformity, and (c) enlargement.

3D deformation measurement system. This system uses a digital image correlation algorithm to match deformation points on the object surface. Based on the parallax data of each point and the pre-calibrated obtained camera parameters, the 3D coordinates of the object surface points were rebuilt.[37] As shown in Figure 7(a), a square reference subset of (2M + 1)*(2M + 1) pixels centered on point "C" was picked up in the reference image. The matching process was to find the corresponding subset centered on point "C" in the deformed image. Therefore, the center points "C" and "C′," "P" and "P′" represent the corresponding points before and after deformation. The corresponding subset positions can be determined by searching for the maximum or minimum in the specified area. The speckle image of the basement membrane of the culture chamber is shown in Figure 7(c), which was made by spraying with matte black paint. The color of the edges of the membrane of the chamber in Figure 7(c) was lighter, which may affect the measurement result. The uneven spraying of spots on both sides of the chamber in Figure 7(e) can lead to errors in speckle recognition. The camera did not recognize the speckles on the membrane due to the excessive spraying of spots in the chamber in Figure 7(f). Therefore, the chamber in Figure 7(d) was selected as the sample in this experiment. It had uniform speckles and optimal color contrast, which can keep the accuracy of image matching, and the size of the spots was the same to avoid the jumping phenomenon.

Results

Three structures of culture chamber with "M"-type optimized profile

The basement membrane shapes of three chambers were obtained based on the optimization results by finite-element simulations. The change trends have a high similarity. The thickness of the middle area of the membrane is larger, along the longitudinal decrease sequentially and then increases at the side. Figure 8 shows the "M"-type thickness profile of the optimized chamber. The upper and lower surfaces of the membrane before optimization are planar with constant thicknesses "t" of 0.5 and 1 mm, respectively. To achieve strain uniformity, the "t" value is continuously changed by optimization iterations. The membrane with a flat upper surface and a curved lower surface exhibited an "M"-type profile after optimization, and the strain field on the membrane surface was more uniform.

The optimization results showed that the strain uniformities of the surface of the three chambers membrane were substantially improved. As shown in Figure 9, the optimized

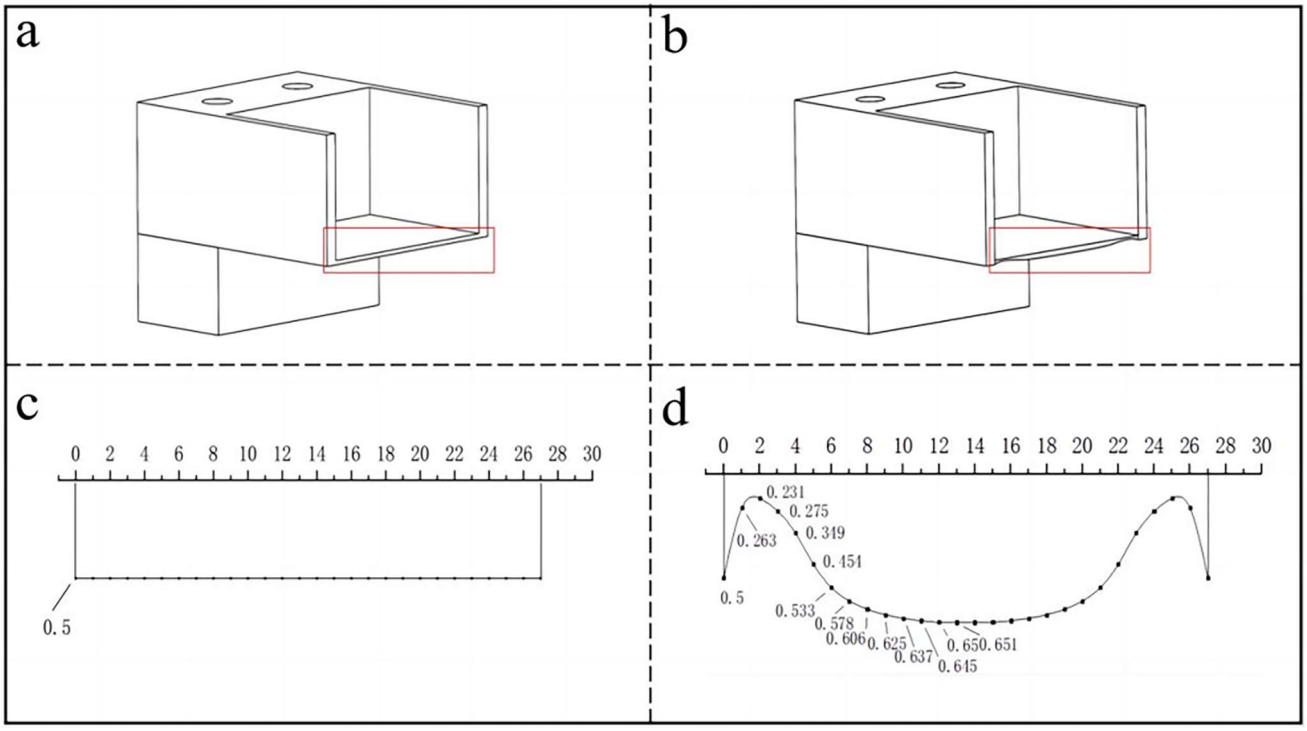

Figure 5. Optimized design model of double-column symmetrical structure (Double-0.5 chamber) culture chamber with 0.5 mm basement membrane thickness and coordinate diagram under 1% strain: (a) basement membrane contour before optimization, (b) the optimized basement membrane contour, (c) thickness coordinate of basement membrane before optimization, and (d) thickness coordinate of optimized basement membrane.

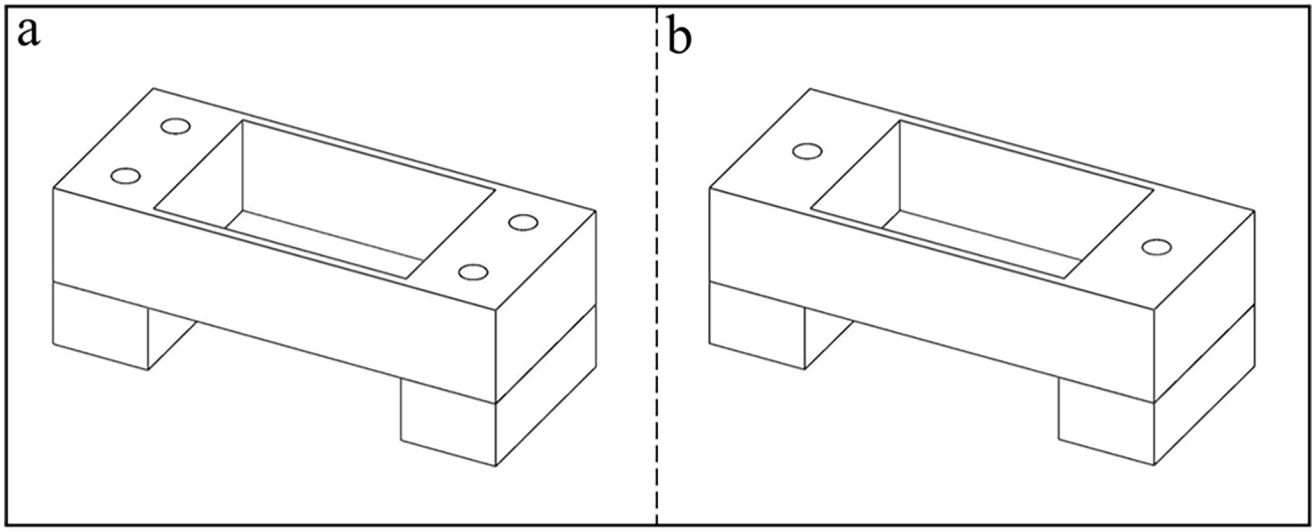

Figure 6. Three-dimensional model of culture chamber: (a) a double-column symmetrical structure (Double-1 chamber) with a basement membrane thickness of 1 mm and (b) a single-column symmetrical structure with a basement membrane thickness of 0.5 mm (Single-0.5 chamber).

Double-1 chamber membrane obtained an effective strain at the surround, increasing the utilization of the membrane. The Single-0.5 chamber membrane before optimization made the strain value fluctuate greatly during loading, and it was not easy to reach the predetermined value. However, the strain values were more stable after optimization. The optimized structure further improved strain accuracy and stability.

In summary, the strain uniformity factor $\gamma(5\%)$ of the three chambers was significantly improved after optimization. Strain uniformity varies with the central longitudinal strain, which means that the strain uniformity changes during loading. As shown in Figure 10, the optimized Double-1 chamber has the largest $\gamma(5\%)$ value. The optimization further improved the $\gamma(5\%)$ value and increased the accuracy of the values, which ensured that the strain was within the allowable error range during loading. The small $\gamma(5\%)$ value of the Single-0.5 chamber before optimization indicated poor structure adaptability.

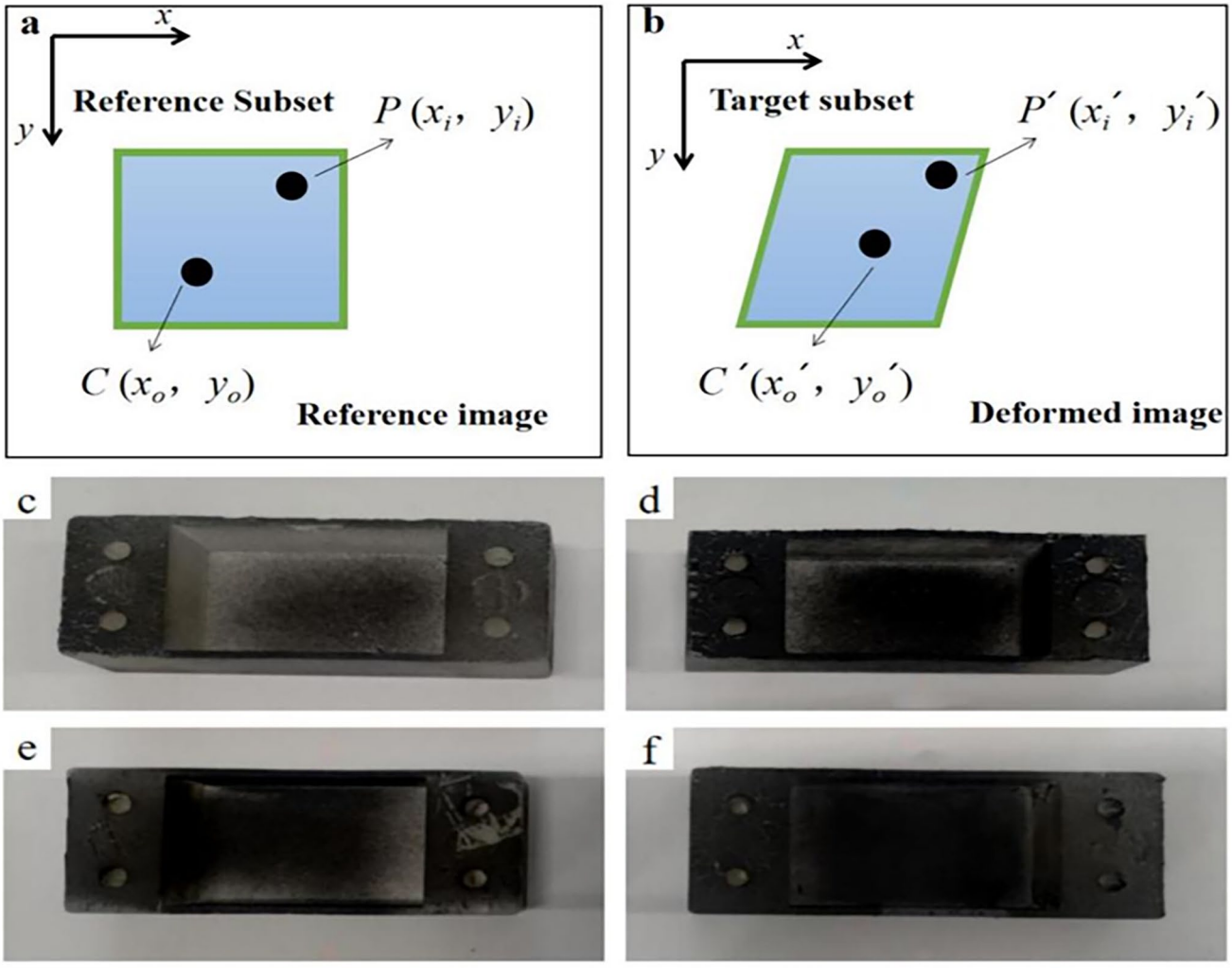

Figure 7. DIC measurement system principle and speckle image: (a) the reference image, (b) the deformed image, (c) the light color of the sprayed matte black paint at the edge of the basement membrane of the chamber and the small color contrast affect the experimental results, (d) the scattering spots on the basement membrane of the chamber are uniform, which maintains the accuracy of image matching, (e) the color of the black paint sprayed on one side of the chamber basement membrane is darker and lighter on the other side, which affects image recognition, and (f) too much black paint is sprayed on the chamber basement membrane, the color is darker, and the spots are not identified.

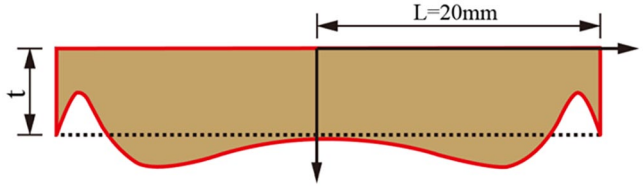

Figure 8. Profile of "M"-type thickness of the chamber membrane.

However, the $\gamma(5\%)$ value significantly improved after optimization and compensated for the problems of the original structure, which can be reasonably selected according to the laboratory conditions. The optimized Double-0.5 chamber also improved the $\gamma(5\%)$ value, with the improvement being more pronounced at small strain and decreasing as strain increases. After optimization, the Double-1 chamber $\gamma(5\%)$ value raised from 0.6722 to 0.9022, an increase of 23%. The Single-0.5 chamber $\gamma(5\%)$ value increased from 0.3368 to 0.6775, an increase of 34.07%. Furthermore, the Double-0.5 chamber $\gamma(5\%)$ value increased from 0.6561 to 0.784, an increase of 12.79%. These results demonstrated the feasibility of the optimization method and improved strain uniformity of the chambers.

Optimized chamber was manufactured

The optimized chamber models was used to establish by SolidWorks (Dassault, USA) software. Due to the low stiffness and strength of resin mold material prepared by 3D printing technology, it is easy to have defects such as mold surface paint chipping, de-molding difficulties, and loading pile fractures. Therefore, according to ASTM standards, A283 material was used to prepare the chamber mold. The mold was fabricated using CNC precision milling, and the surface was polished and painted with a roughness of Ra0.8. This method can ensure high surface quality and transparency after forming the chamber. As shown in Figure 11, the positioning column was designed

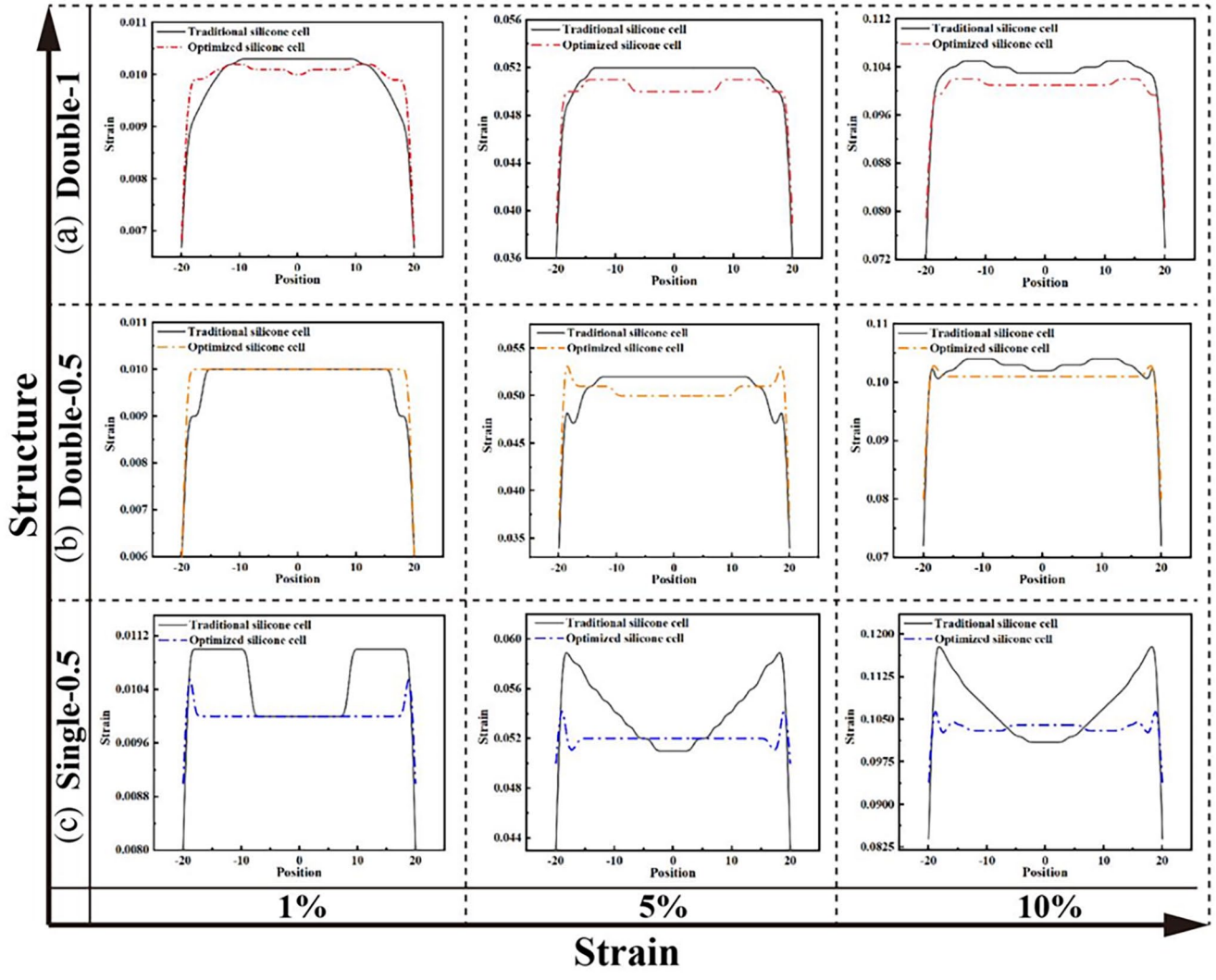

Figure 9. Strain field of membrane top before and after optimization under 1%, 5%, and 10% strain of culture chamber with three structures: (a) to (c) strain field at the top of the membrane before and after optimization at 1%, 5%, and 10% strain in Double-1 chamber; (d) to (f) strain field at the top of the membrane before and after optimization at 1%, 5%, and 10% strain in Double-0.5 chamber; and (g) to (i) strain field at the top of the membrane before and after optimization at 1%, 5%, and 10% strain in Single-0.5 chamber.

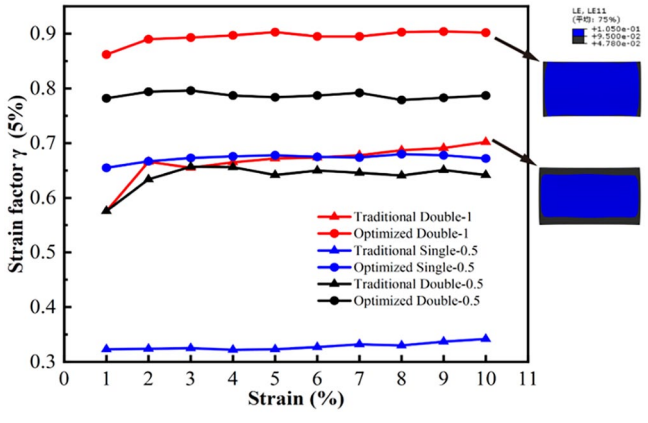

Figure 10. $\gamma(5\%)$ value change rule of three structures before and after optimization under different strains.

to be removable for easy de-molding, thus reducing friction and damage to the chamber.

Experiment results

The Double-1 chamber was subjected to a 3D digital image experiment using high-precision cameras to measure the strain field distribution of the membrane at 1%, 5%, and 10% strains. As shown in Figure 12, the strain field distribution on the membrane was verified; the experimental results demonstrated high consistency with the numerical simulations, which substantiates the rationality of the optimized chamber.

Discussion

This study improved the problem of non-uniformity strain on the chamber membrane during loading. Gilbert et al. studied the strain of the membrane under pressure, whose results indicated that achieving a more uniform strain was difficult when using either too-thick or too-thin membranes.[33] Wang et al. explored the effect of profile thickness variation in column-free circular elastic membranes to study the

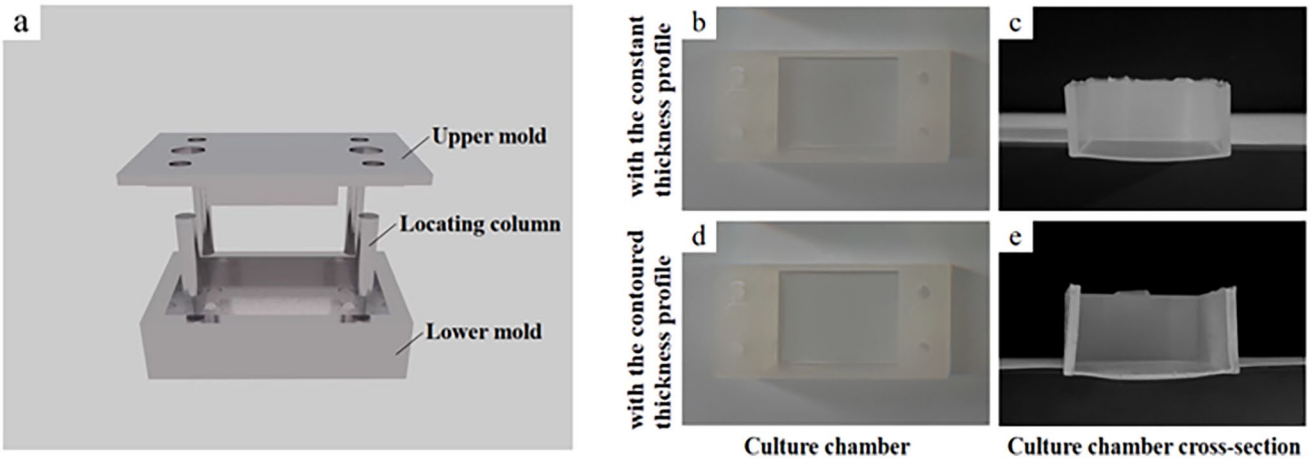

Figure 11. Manufacturing process: (a) culture chambers with the desired thickness profile were prepared using a multi-step replica molding process, (b) culture chambers with the constant thickness profile, (c) the thickness of the longitudinal profile of the membrane is constant, (d) culture chambers with the contoured thickness profile, and (e) the thickness of the longitudinal profile of the membrane is "M" type.

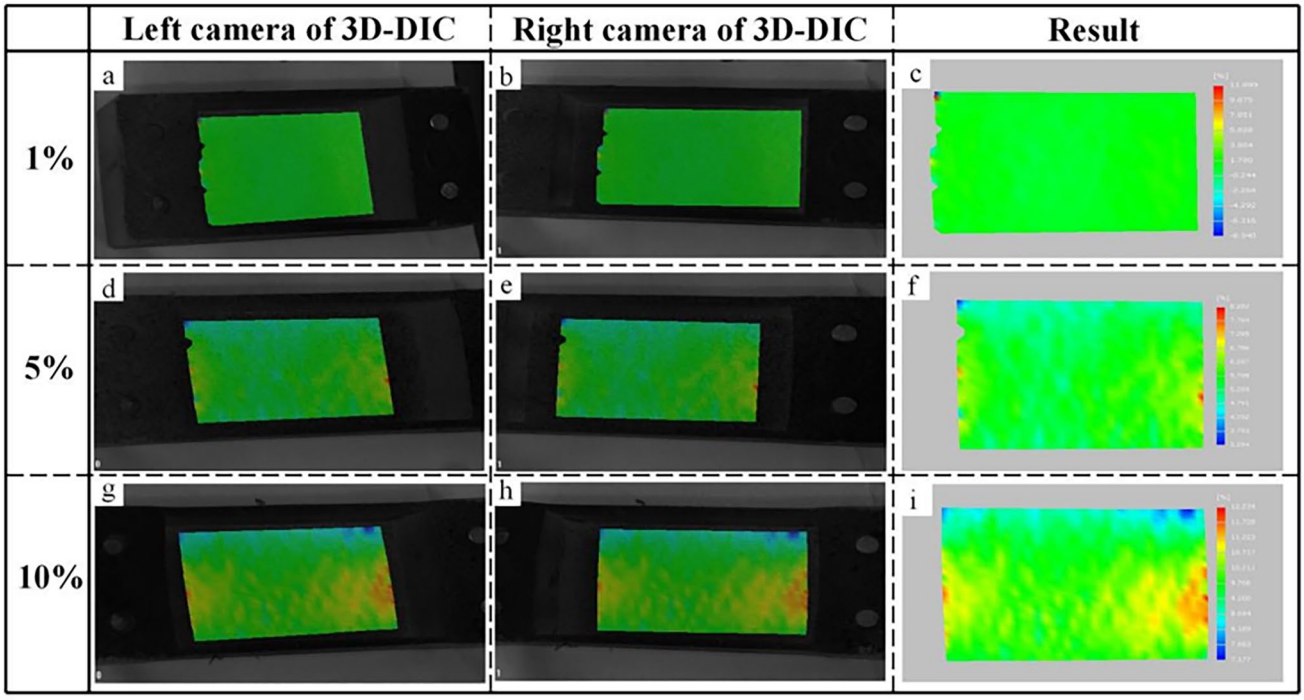

Figure 12. Comparison between quantitative analysis and numerical simulation of membrane strain calculated by DIC method: (a) to (c) strain field distribution at 1% strain for 3D-DIC experiments performed with double high-precision cameras on basement membrane; (d) to (f) strain field distribution at 5% strain for 3D-DIC experiments performed with double high-precision cameras on basement membrane; and (g) to (i) strain field distribution at 10% strain for 3D-DIC experiments performed with double high-precision cameras on basement membrane.

uniformity of radial strain. Four structures were designed by varying the thickness and height of the membranes, and the results showed that the new structures lacked a theoretical basis, although they improved the uniform strain.[38] Cell tensile experiments were carried out with a cell loading device and culture chamber developed in this article; after 60 h of stretching, cells with crystal violet staining were observed under a 40× and 100× microscope, as shown in Figure 13. The results showed that the cell growth density was relatively uniform, which proved that the device could produce a certain loading effect on cell mechanics and provided conditions for the research of cell mechanobiology.

This article optimized three "M" structure membranes based on the finite-element method. During the iterative process, node positions on the lower surface of the membrane were adjusted until the strain value on the upper surface of the membrane remained constant, reducing partial stress concentration and enhancing strain uniformity. The proposed optimization method can be applied to various strain conditions. The experiment verified the rationality of

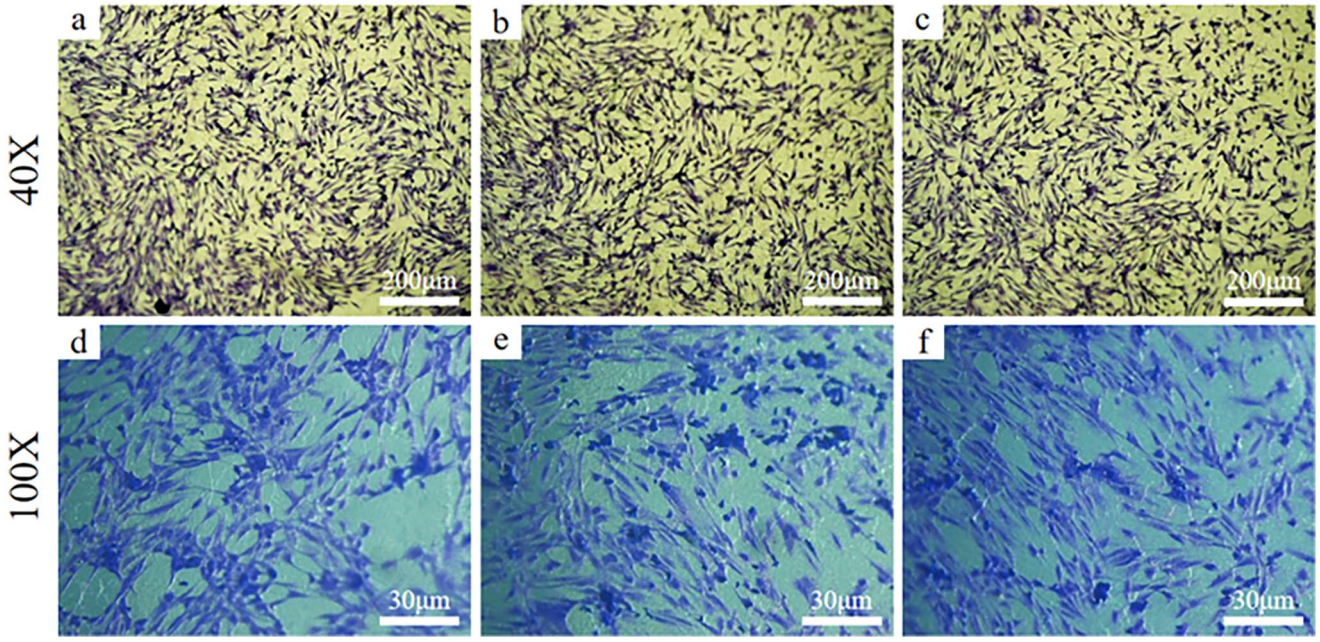

Figure 13. Micrograph of cell tensile loading: (a) to (c) cell changes after 60 h of stretching under a 40× microscope; (d) to (f) cell changes after 60 h of stretching under a 100× microscope.

the optimization, which the variation of membrane thickness with strain and the thickness would not interfere with the optical measurement.[17]

Furthermore, the strain uniformity factor is combined to better analyze the strain situation of the three chambers basement membrane. The results showed that the Double-1 chamber generated a more uniform strain field and enhanced the strain uniformity factor up to 90%. In contrast, the Single-0.5 chamber exhibited stress concentration due to the single-column stretching, and excessive longitudinal strain led to significant vertical contraction, resulting in inferior strain uniformity; however, the strain uniformity factor can still be improved to 67.75% after optimization. Currently, Double-0.5 chambers are more commonly employed in applications. The double-column structure facilitates a more secure fixation of the chambers, minimizing the deflection of the fixed end during loading. The applied displacement load is more uniformly distributed to the membrane, preventing excessive partial strain and increasing the precision of the experiment. In addition, the overall structure is more adaptable.

Conclusions

In this article, a culture chamber with an "M" profile structure has been obtained that can transmit uniform uniaxial strain to cultured cells *in vitro*. This chamber was poured using a multi-step molding process. The strain uniformity of the membrane was quantified according to the strain uniformity factor. Among the three structures, the strain uniformity factor of the Double-1 chamber could reach 0.90, and the strain uniformity area was more extensive, which could be applied in cell mechanobiological experiments. The 3D-DIC experiments showed that culture chambers with an "M"-type profile structure could generate a larger strain field area during loading than chambers with a constant thickness membrane. Therefore, the culture chambers using the cell loading device with an "M"-profile structure could help improve the accuracy when cell regulation and adaptation mechanisms are mechanobiological researched. This article provides a robust theoretical and experimental foundation for biomechanics-related research.

AUTHORS' CONTRIBUTION

All authors participated in the design, interpretation of the studies, and analysis of the data and review of the manuscript. XTG and ZQW conducted experiments. LLG and CQZ conducted simulations. XTG and ZQW wrote the manuscript, and CQZ reviewed the manuscript.

ACKNOWLEDGEMENTS

The authors thank Prof. Xunwei Wu's group at Shandong University Dental Hospital for support in biological test.

DECLARATION OF CONFLICTING INTERESTS

The author(s) declared no potential conflicts of interest with respect to the research, authorship, and/or publication of this article.

FUNDING

The author(s) disclosed receipt of the following financial support for the research, authorship, and/or publication of this article: This work was supported by the National Natural Science Foundation of China (grant nos. 12072235 and 32271371) and the Natural Science Foundation of Tianjin City (grant no. 21JCYBJC00940).

ORCID ID

Xutong Guo https://orcid.org/0000-0002-3614-4298

SUPPLEMENTAL MATERIAL

Supplemental material for this article is available online.

REFERENCES

1. Choi Y, Morlino G, Toboso-Navasa A, Hopf R, Pramotton FM, Bigot A, Taddei A, Cesarovic N, Falk V, Mazza E, Giampietro C. A novel bistable device to study mechanosensitive cell responses to instantaneous stretch. *Biomater Adv* 2022;**141**:213134
2. Branecka N, Lekszycki T. Experimental methods of living cells mechanical loading: review. *Continuum Mech Thermodyn* 2022;**35**:1165–1183
3. Kolel A, Ergaz B, Goren S, Tchaicheeyan O, Lesman A. Strain gradient programming in 3D fibrous hydrogels to direct graded cell alignment. *Small Methods* 2022;**7**:2201070
4. Happe CL, Engler AJ. Mechanical forces reshape differentiation cues that guide cardiomyogenesis. *Circ Res* 2016;**118**:296–310
5. Aragona M, Panciera T, Manfrin A, Giulitti S, Michielin F, Elvassore N, Dupont S, Piccolo S. A mechanical checkpoint controls multicellular growth through YAP/TAZ regulation by actin-processing factors. *Cell* 2013;**154**:1047–59
6. Beloussov LV, Saveliev SV, Naumidi II, Novoselov VV. Mechanical stresses in embryonic tissues: patterns, morphogenetic role, and involvement in regulatory feedback. *Int Rev Cytol* 1994;**150**:1–34
7. Simpson DG, Carver W, Borg TK, Terracio L. Role of mechanical stimulation in the establishment and maintenance of muscle cell differentiation. *Int Rev Cytol* 1994;**150**:69–94
8. Pfister BJ, Grasman JM, Loverde JR. Exploiting biomechanics to direct the formation of nervous tissue. *Curr Opin Biomed Eng* 2020;**14**:59–66
9. Brown TD. Techniques for mechanical stimulation of cells in vitro: a review. *J Biomech* 2000;**33**:3–14
10. Chen JH, Liu C, You L, Simmons CA. Boning up on Wolff's law: mechanical regulation of the cells that make and maintain bone. *J Biomech* 2010;**43**:108–18
11. Sears C, Kaunas R. The many ways adherent cells respond to applied stretch. *J Biomech* 2015;**49**:1347–54
12. Meng LD, Xue GL, Liu QJ, Xie TP, Fan D, Gou X. In-situ electromechanical testing and loading system for dynamic cell-biomaterial interaction study. *Biomed Microdevices* 2020;**22**:56
13. Dai ZX, Shih PJ, Yen JY, Wang IJ. Functional assistance for stress distribution in cell culture membrane under periodically stretching. *J Biomech* 2021;**125**:110564
14. Zhang C, Qiu L, Gao L, Guan Y, Xu Q, Zhang X, Chen Q. A novel dual-frequency loading system for studying mechanobiology of load-bearing tissue. *Mater Sci Eng C Mater Biol Appl* 2016;**69**:262–7
15. Van Dyke WS, Sun X, Richard AB, Nauman EA, Akkus O. Novel mechanical bioreactor for concomitant fluid shear stress and substrate strain. *J Biomech* 2012;**45**:1323–7
16. Bianchi F, George JH, Malboubi M, Jerusalem A, Thompson MS, Ye H. Engineering a uniaxial substrate-stretching device for simultaneous electrophysiological measurements and imaging of strained peripheral neurons. *Med Eng Phys* 2019;**67**:1–10
17. Apa L, Carraro S, Pisu S, Peruzzi B, Rizzuto E, Prete ZD. Development and validation of a device for in vitro uniaxial cell substrate deformation with real-time strain control. *Meas Sci Technol* 2020;**31**:125702
18. Shimizu K, Shunori A, Morimoto K, Hashida M, Konishi S. Development of a biochip with serially connected pneumatic balloons for cell-stretching culture. *Sens Actuators B Chem* 2011;**156**:486–93
19. Sato K, Kamada S, Minami K. Development of microstretching device to evaluate cell membrane strain field around sensing point of mechanical stimuli. *Int J Mech Sci* 2010;**52**:251–6
20. Kim TK, Jeong OC. Fabrication of a pneumatically-driven tensile stimulator. *Microelectro Eng* 2012;**98**:715–9
21. Masuda T, Takahashi I, Anada T, Arai F, Fukuda T, Takano-Yamamoto T, Suzuki O. Development of a cell culture system loading cyclic mechanical strain to chondrogenic cells. *J Biotechnol* 2008;**133**:231–8
22. Lei Y, Masjedi S, Ferdous Z. A study of extracellular matrix remodeling in aortic heart valves using a novel biaxial stretch bioreactor. *J Mech Behav Biomed Mater* 2017;**75**:351–8
23. Dermenoudis S, Missirlis Y. Design of a novel rotating wall bioreactor for the in vitro simulation of the mechanical environment of the endothelial function. *J Biomech* 2010;**43**:1426–31
24. Toume S, Gefen A, Weihs D. Printable low-cost, sustained and dynamic cell stretching apparatus. *J Biomech* 2016;**49**:1336–9
25. Tsukamoto S, Asakawa T, Kimura S, Takesue N, Mofrad MRK, Sakamoto N. Intranuclear strain in living cells subjected to substrate stretching: a combined experimental and computational study. *J Biomech* 2021;**119**:110292
26. Morita Y, Watanabe S, Ju Y, Yamamoto S. In vitro experimental study for the determination of cellular axial strain threshold and preferential axial strain from cell orientation behavior in a non-uniform deformation field. *Cell Biochem Biophys* 2013;**67**:1249–59
27. Bieler FH, Ott CE, Thompson MS, Seidel R, Ahrens S, Epari DR, Wilkening U, Schaser KD, Mundlos S, Duda GN. Biaxial cell stimulation: a mechanical validation. *J Biomech* 2009;**42**:1692–6
28. Rubin CT, Lanyon LE. Regulation of bone mass by mechanical strain magnitude. *Calcif Tissue Int* 1985;**37**:411–7
29. Balachandran K, Alford PW, Wylie-Sears J, Goss JA, Grosberg A, Bischoff J, Aikawa E, Levine RA, Parker KK. Cyclic strain induces dual-mode endothelial-mesenchymal transformation of the cardiac valve. *Proc Natl Acad Sci USA* 2011;**108**:19943–8
30. Rana OR, Zobel C, Saygili E, Brixius K, Gramley F, Schimpf T, Mischke K, Frechen D, Knackstedt C, Schwinger RH, Schauerte P, Saygili E. A simple device to apply equibiaxial strain to cells cultured on flexible membranes. *Am J Physiol Heart Circ Physiol* 2008;**294**:H532–140
31. Bottlang M, Simnacher M, Schmitt H, Brand RA, Claes L. A cell strain system for small homogeneous strain applications. *Biomed Tech (Berl)* 1997;**42**:305–9
32. Sotoudeh M, Jalali S, Usami S, Shyy JY, Chien S. A strain device imposing dynamic and uniform equi-biaxial strain to cultured cells. *Ann Biomed Eng* 1998;**26**:181–9
33. Gilbert JA, Weinhold PS, Banes AJ, Link GW, Jones GL. Strain profiles for circular cell culture plates containing flexible surfaces employed to mechanically deform cells in vitro. *J Biomech* 1994;**27**:1169–77
34. Wang Z, Gao L, Lyu L, Wang X, Zhang C. [Development of a culture chamber for mechanical loading of adherent cells with large uniform strain]. *Sheng Wu Yi Xue Gong Cheng Xue Za Zhi* 2022;**39**:997–1004
35. Cui L, Wang X, Gao L, Zhang C, Zhang X. Development of strain loading device for adherent cells in vitro. *J Med Biomech* 2020;**35**:568–73
36. Vande Geest JP, Di Martino ES, Vorp DA. An analysis of the complete strain field within FlexercellTM membranes. *J Biomech* 2004;**37**:1923–8
37. Yang M, Xiang D, Wang S. The radial bulging and axial strains of intervertebral discs during creep obtained with the 3D-DIC system. *Biomolecules* 2022;**12**:1097
38. Wang Q, Huang H, Niu Y, Zhang X, Jiang P, Swindle-Reilly KE, Zhao Y. Microscale cell stretcher to generate spatially uniform equi-biaxial strain using an elastomeric membrane with a contoured thickness profile. *Sensors Actuators B: Chem* 2018;**273**:1600–9

(Received February 1, 2023, Accepted June 7, 2023)